

# JUNGFRAU

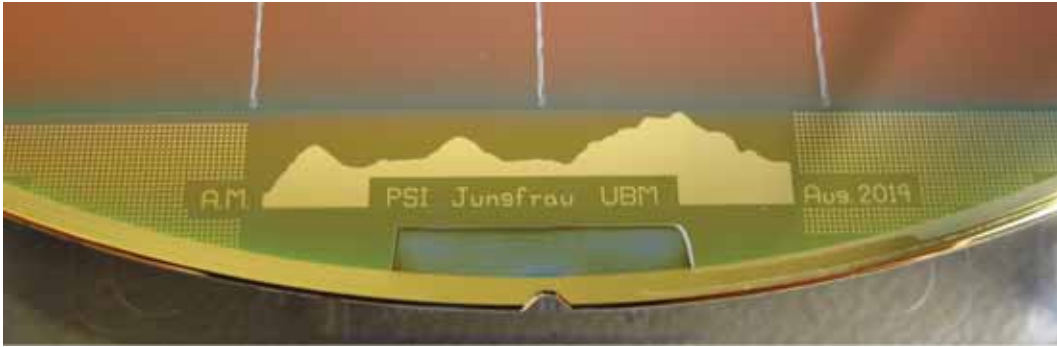
## A Dynamic Gain Switching Detector for SwissFEL

### Technical Design Report

Julia H. Smith, Aldo Mozzanica, Bernd Schmitt

Swiss Light Source Detector Group  
Paul Scherrer Institut, Villigen PSI, Switzerland

January 2015



#### Abstract

*JUNGFRAU (adJUstiNg Gain detector FoR the Aramis User station) is a two-dimensional pixel detector for photon science applications at free electron lasers (FEL) and synchrotron light sources. It is developed for the SwissFEL facility currently under construction at the Paul Scherrer Institute, Switzerland. Distinguishing characteristics of the detection system include single photon sensitivity and a low noise performance over a dynamic range of over four orders of magnitude of input signal. These characteristics are achieved by a three-fold gain-switching preamplifier in each pixel, which automatically adjusts its gain to the amount of charge deposited on the pixel. Geometrically, the final JUNGFRAU chip comprises  $256 \times 256$  pixels of  $75 \times 75 \mu\text{m}^2$  each. The chips are coupled to silicon sensors. Arrays of  $2 \times 4$  chips are tiled to form modules of about  $4 \times 8 \text{ cm}^2$ . Multi-module systems up to 16 MPixel are planned for the two end stations at SwissFEL. A readout rate in excess of 2 kHz is anticipated, which serves the readout requirements of SwissFEL and enables high count rate synchrotron experiments with a linear count rate capability of 20 MHz/pixel. Details and selected characterization results from both JUNGFRAU 0.1 and JUNGFRAU 0.2 are presented with a focus on characterization results from the second JUNGFRAU prototype chip. ASIC characterization results as well as detector tests from the hybridized chip under white visible light, fluorescence X-ray, infrared laser and synchrotron irradiation are presented.*

# Contents

<b>1</b>	<b>Introduction</b>	<b>3</b>
1.1	The SwissFEL Project . . . . .	3
1.2	Overview of Current Detector Developments for XFELs and Synchrotrons . . . . .	3
<b>2</b>	<b>JUNGFRAU</b>	<b>5</b>
2.1	General Detector Design . . . . .	5
2.2	Detector Geometry . . . . .	5
2.3	ASIC Design . . . . .	7
2.3.1	Pixel Design . . . . .	8
2.3.2	Periphery and Readout Architecture . . . . .	9
2.4	Detector Integration . . . . .	11
2.5	Prototypes . . . . .	11
2.5.1	JUNGFRAU 0.1 . . . . .	11
2.5.2	JUNGFRAU 0.2 . . . . .	11
<b>3</b>	<b>Envisioned Systems for SwissFEL</b>	<b>13</b>
3.1	JUNGFRAU for ES-A . . . . .	13
3.2	JUNGFRAU for ES-B . . . . .	13
3.3	JUNGFRAU for SwissFEL “Pool” . . . . .	14
3.4	JUNGFRAU Production . . . . .	14
<b>4</b>	<b>Characterization Results</b>	<b>15</b>
4.1	Noise Performance and Photon Detection at Low Energies . . . . .	15
4.2	Photon Detection above 10 keV . . . . .	18
4.3	Gain . . . . .	18
4.4	Linearity of the Pixel Response . . . . .	19
4.5	Speed . . . . .	20
4.6	Imaging Measurements . . . . .	21
4.6.1	High Dynamic Range Imaging Via Gain Switching . . . . .	21
4.6.2	Spatial Imaging Resolution . . . . .	24
<b>5</b>	<b>Project Milestones and Future Timeline</b>	<b>25</b>
<b>6</b>	<b>The JUNGFRAU Team</b>	<b>26</b>
<b>7</b>	<b>Concluding Remarks and Outlook</b>	<b>27</b>
	<b>Further Information</b>	<b>27</b>
	<b>Acknowledgements</b>	<b>27</b>
	<b>References</b>	<b>28</b>

# 1 Introduction

## 1.1 The SwissFEL Project

At present, a new generation X-ray source, the “SwissFEL” [1, 2] X-ray free electron laser (XFEL), is under construction at the Paul Scherrer Institute (PSI) in Villigen, Switzerland. This light source represents one of currently four XFEL projects, which deliver hard X-ray pulses at wavelengths down to 1 Å [1].

The properties of SwissFEL will enable the investigation of ultrafast processes and interactions in molecular systems on the Ångström length scale. Examples of the science drivers for SwissFEL include but are not limited to the study of reaction chemistry, catalysis, material sciences, novel materials and nanostructures [1, 2, 3].

The SwissFEL hard X-ray beam line, Aramis, initially comprises two experimental stations (ES), ES-A and ES-B. ES-A will be a “general purpose” pump-probe experimental station which will provide experimental capabilities for X-ray spectroscopy, including techniques like X-ray absorption (XAS), X-ray emission (XES), resonant inelastic X-ray scattering (RIXS), X-ray diffuse scattering, femtosecond serial nanocrystallography and X-ray diffraction on molecular crystals [4]. ES-B will be an experimental station for femtosecond X-ray pump-probe diffraction and scattering featuring experimental techniques such as time-resolved X-ray diffraction (trXRD), time-resolved resonant X-ray diffraction (trRXRD) and time-resolved resonant inelastic X-ray scattering (trRIXS) [5].

The characteristics of the SwissFEL machine and of the scientific experiments at ES-A [4] and ES-B [5] impose specific requirements for dedicated detector technology. These translate into a two-dimensional (2D), modular and tilable, vacuum-compatible imaging detector with pixel sizes comparable to state-of-the-art photon counting detectors, single photon sensitivity for energies  $> 2$  keV, low noise and good linearity of detection over the full dynamic range, a high dynamic range with up to  $10^4$  12 keV photons per pulse per pixel, and frame rates in excess of 100 Hz.

## 1.2 Overview of Current Detector Developments for XFELs and Synchrotrons

Few dedicated detection systems are under development for photon science at these brilliant light sources. Importantly, single photon counting detectors (like PILATUS [6], EIGER [7] or Medipix [8]) are not suitable for the high photon fluxes at XFEL. The use of charge-integrating detection systems becomes crucial. Each of these new detection systems for XFELs is tailored to meet the specific requirements of their respective light source. These detector systems comprise the Cornell-SLAC Pixel Array Detector (CSPAD) [9] for the SLAC Linac Coherent Light Source (LCLS, Stanford, USA) [10], the Adaptive Gain Integrating Pixel Detector (AGIPD) [11], the Large Pixel Detector (LPD) [12] and the DEPFET Sensor with Signal Compression (DSSC) [13] for the European X-ray Free Electron Laser (EU-XFEL, Hamburg, Germany) [14] and the Silicon-On-Insulator PHoton Imaging Array Sensor (SOPHIAS) [15] for the SPring-8 Angstrom Compact free electron LASer (SACLA, Harima, Japan) [16].

None of the mentioned detection systems is capable to serve the specific needs of the SwissFEL experiments (Table 1), in particular, the requirements for two-dimensional detection systems of the Aramis beam line and its user stations ES-A [4] and ES-B [5]. Therefore, a dedicated, state-of-the-art application-specific integrated circuit (ASIC) and detector system is being developed for photon science applications at PSI: JUNGFRÄU, the adJUstiNg Gain detector FoR the Aramis User station [17].

In addition, high count rate synchrotron experiments could largely benefit from these new detector developments for XFEL light sources. Detection systems with a high count rate capacity are

particularly interesting to synchrotron applications that are currently rate limited. Examples include protein crystallography experiments where often only about 2 to 10% of the available photon flux is used for experiments to avoid detector saturation [18]. Novel high dynamic range detector systems enable a more efficient use of the available photon flux and hence greatly reduce the measurement time. XFEL detector systems like JUNGFRÄU meet the requirements of many synchrotron applications and complement the existing photon counting systems with high photon rate capabilities.

Detector System	Pixel Size [ $\mu\text{m} \times \mu\text{m}$ ]	Noise [ $e^-$ ]	Single Photon Sensitivity	Dynamic Range*	Repetition Rate [kHz]
CSPAD	110×110	330	Yes. <sup>‡</sup>	$2.5 \cdot 10^3$ (@ 8keV)	0.12
AGIPD	200×200	265	Yes.	$>10^4$ (@12 keV)	4500
LPD	500×500	1000	No.	$10^5$	4500
DSSC	Pitch 200 <sup>†</sup>	50	Yes.	$>6 \cdot 10^3$ (@1 keV)	1000-5000
SOPHIAS	30×30	150	TBD	TBD	0.06
JUNGFRÄU	75×75	100	Yes.	$>10^4$ (@ 12 keV)	0.1-2.4

<sup>†</sup> Hexagonal pixel shape.

<sup>‡</sup> CSPAD has two user-configurable gain stages: Single photon resolution with a small dynamic range or up to 2500 photons without single photon discrimination.

\* Dynamic Range refers to the maximum number of photons which can be detected per pixel per pulse.

Table 1: Comparison of the main characteristics of the current state-of-the-art pixelated detection systems for the XFEL hard X-ray light sources. Cells colored in red indicated design characteristics which limit the applicability of the particular detection system to SwissFEL, while green cells highlight performance characteristics in accordance with the experimental requirements of the SwissFEL user end stations.

## 2 JUNGFRAU

### 2.1 General Detector Design

The detector requirements of SwissFEL and its envisioned experiments (as described in 1.1) translate directly into the JUNGFRAU design and performance characteristics. The development of the JUNGFRAU detector reuses, whenever possible, design blocks which have already been developed and successfully been used for other PSI detectors in order to minimize the development time and to keep the project cost at an affordable level.

JUNGFRAU is a charge-integrating detector rather than a single photon counter. Most hybrid pixel detectors for synchrotron radiation are based on the photon counting principle which cannot meet the requirements of XFEL applications. In photon counting detectors, an event in the sensor causes a response in one or more ASIC pixels. Whenever such a response pulse reaches a user-set threshold level in a photon counting ASIC, the event is “counted”. Photon counting is inaccurate when photons arrive at the detector the same time or when photon events are piled-up. Charge integrating ASICs record a charge proportional to the signal pulse created by an event in the sensor. The integrated charge is proportional to the number of events, i.e. the number of photons interacting with the sensor, for monochromatic light.

### 2.2 Detector Geometry

Geometrically, the final JUNGFRAU chip comprises  $256 \times 256$  pixels of  $75 \times 75 \mu\text{m}^2$  each. Arrays of  $2 \times 4$  chips ( $512 \times 1024$  pixels) are tiled to form modules of  $38.4 \times 76.8 \text{ mm}^2$  sensitive area, i.e. about 500 kPixel per module (Figure 1). The chips are coupled to  $320 \mu\text{m}$  or  $450 \mu\text{m}$  thick p+ on n silicon sensors (Hamamatsu Photonics, Hamamatsu, Japan), which have the same characteristics as the ones used for EIGER [7]. The dimensions of the module mechanics are also derived from the EIGER project (Figure 2 and 3). Small modification are required to adapt the modules to the different readout electronics and for vacuum compatibility. Multi-module systems of 1 MPixel (2 modules), 4 MPixel (8 modules, Figure 1), 8 MPixel (16 modules)/9 MPixel (18 modules), 16 MPixel (32 modules) are envisioned and can be tiled in application-specific geometries. The gap between two adjacent JUNGFRAU modules is about  $500 \mu\text{m}$ , which corresponds to an insensitive area of about 7 pixels. Section 3 briefly outlines the systems planned for the experimental setups at the two end stations of SwissFEL.

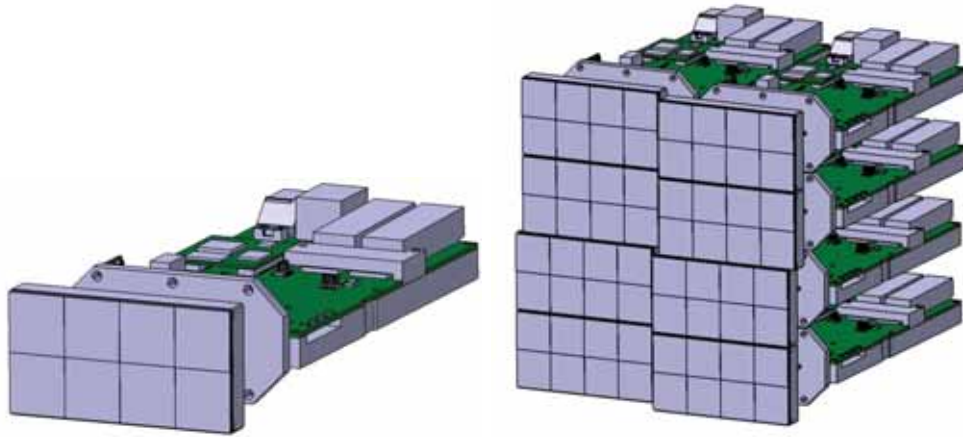


Figure 1: (left) A single JUNGFRAU module consisting of  $2 \times 4$  chips, i.e. 0.5 kPixel. The readout electronics is mounted perpendicular to the pixel plane in a “T-configuration”. The readout system does not extend beyond the detector area such that multiple modules can be tiled to form larger detector systems. (right) A possible geometry for a 4 MPixel JUNGFRAU detection system (8 JUNGFRAU modules) is displayed. The example 4 MPixel system is constructed such that the four detector quadrants are arranged around a small, central recess through which the direct (SwissFEL) beam could pass. The (scattered) photon signal, from e. g. X-ray absorption or X-ray diffraction experiments, is registered in the four detector quadrants.

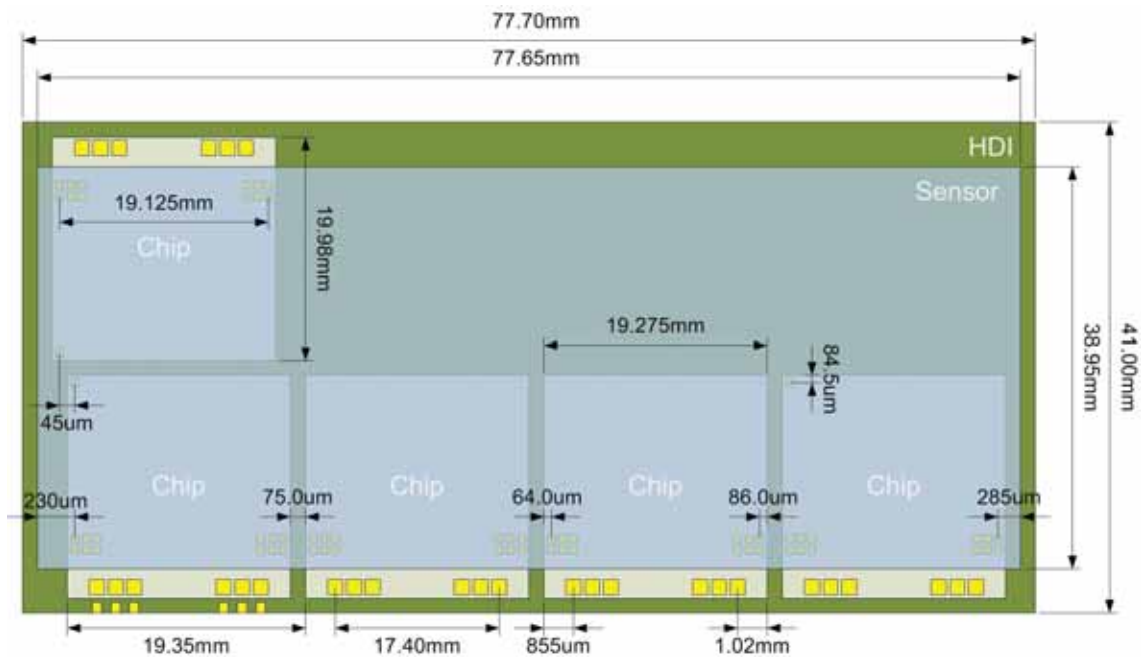


Figure 2: Schematic drawing of the geometry of a JUNGFRAU module (readout board not included, not to scale). Top view of the High Density Interconnect (HDI), the  $256 \times 256$  pixel JUNGFRAU chips, the sensor and the dimensions of/distances between selected components. Figure courtesy Christian Ruder.

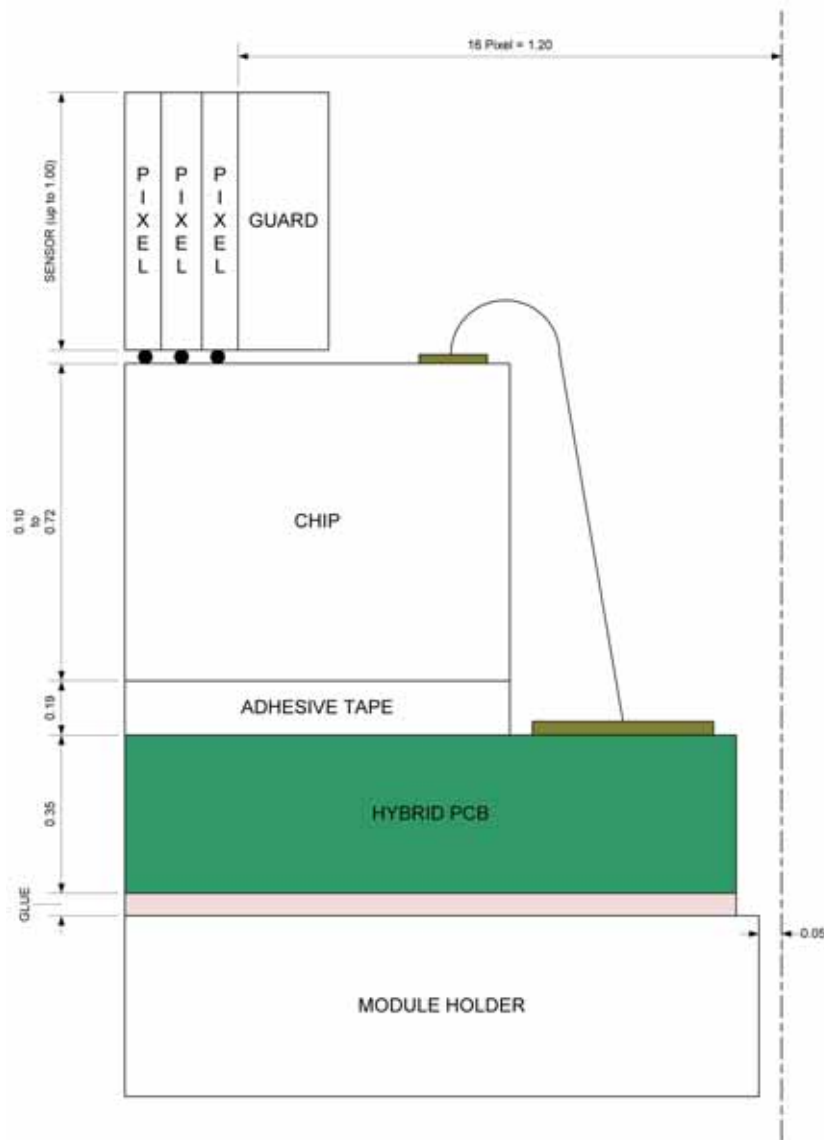


Figure 3: Schematic cross section of the JUNGFRAU module (not to scale). The module holder, the HDI, the JUNGFRAU chip bump-bonded to the sensor and wire-bonds are schematically represented and their dimensions are indicated. Figure courtesy Lukas Schaedler.

### 2.3 ASIC Design

The JUNGFRAU readout chip (ROC) is designed in United Microelectronics Corporation (UMC) 110 nm CMOS technology with Aluminum-only interconnect. The technology is selected for all in-house projects due to the favorable cost-performance ratio, the flexibility and the availability of several multiple project wafer (MPW) runs per year for fast prototyping. Section 2.3.1 and Section 2.3.2 describes the pixel design and the general architecture of the ROC, respectively, while Section 2.5 focuses on the prototype implementation.

### 2.3.1 Pixel Design

The design of the front end block of the JUNGFRAU pixel is very similar to a GOTTHARD channel, which is described in detail in [19]. Reference [19] also covers the working mechanism of the gain switching logic. A schematic view of the pixel circuit is shown in Figure 4. JUNGFRAU consists of several blocks:

- A **preamplifier** with three selectable gains,
- An **automatic gain switching block** consisting of a comparator with tunable threshold and switching control logic,
- A **correlated double sampling (CDS) stage** to remove the preamplifier low frequency and reset noise in high gain,
- A **storage array** for 16 images,
- A **buffer** needed to drive the column bus during the readout phase.

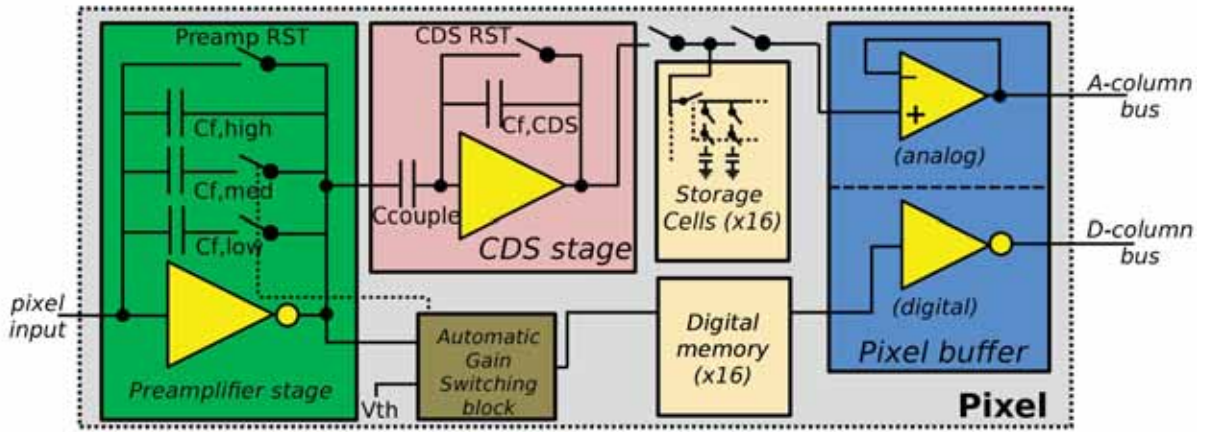


Figure 4: Schematic block diagram of a JUNGFRAU 0.2 pixel.

The main design challenge is the pixel's power budget. As compared to a strip detector like GOTTHARD, the power has to be reduced due to the large increase in the channel density. In particular, the power is reduced from 300-500  $\mu W$  per channel in the GOTTHARD ASIC or the AGIPD designs down to 20-30  $\mu W$  in JUNGFRAU. This power reduction leads to a slower preamplifier and CDS stage. The resulting rise time (Section 4.5) of the JUNGFRAU signals is perfectly adequate for 100 Hz XFEL operation and the envisioned synchrotron applications. A second important consideration in the pixel design is the smaller area available for the preamplifier feedback capacitors. In a  $75 \times 75 \mu m^2$  pixel, the maximum capacitance available for the feedback capacitors is on the order of  $\sim 8$  pF, which is a factor of 2 smaller compared to the components employed in previous designs as AGIPD or GOTTHARD. A precharge scheme for the feedback capacitors has been introduced to still achieve the same dynamic range of  $10^4$  photons per pixel per pulse in a JUNGFRAU pixel: During the preamplifier reset, the output side of the capacitor is not charged to the preamplifier reset level as in the previous designs. Instead, it is set to a tunable voltage level which is chosen such that the preamplifier output is at the lower end of its range for signals just higher than the switching point.

As in the GOTTHARD ROC, the CDS stage is bypassed in case of gain switching. 16 analogue storage cells are present in the pixel, each one with the corresponding 2 bit digital latches to store the gain information. Up to 16 images can be stored on the ROC before readout. The number of storage cells in JUNGFRÄU is a result of area availability after all other functional pixels blocks were laid out (half of the pixel itself) and a storage capacitance of  $\sim 300$  fF was placed. A smaller capacitance value would reduce the linearity performance, since the stored charge will redistribute on the parasitic capacitances of the voltage off-pixel buffer.

### 2.3.2 Periphery and Readout Architecture

The readout of JUNGFRÄU is designed in analogy to the GOTTHARD strip detection system for XFEL applications [17, 19]. JUNGFRÄU readout rates in excess of 2 kHz are anticipated for dead time free operation, which serves the readout requirements of SwissFEL but also enables high count rate synchrotron experiments with a high linear count rate capability of 20 MHz/pixel.

The  $256 \times 256$  pixel matrix of the final ROC will be organized in four super-columns of  $256 \times 64$  pixels, each of which is served by its own off-chip driver. This results in a readout time for the full ASIC of  $256 \times 64 / 40 \text{ MHz} = 410 \mu\text{s}$  where 40 MHz is the design ADC clock speed. This readout time corresponds to a frame rate of about 2 kHz. The chip is read out row-wise: When a row is selected for readout, the output buffer in each pixel is connected to the column bus that drives a second voltage buffer (column buffer) in the periphery. The output of the column buffers is connected to a multiplexer that, at a 40 MHz clock rate, connects one column after the other to the single-end to differential off-chip driver. Since the pixel buffers only need to charge the column bus with the 64 times slower row clock, this two-buffer design enables the use of a low power amplifier in the pixel, and at the same time to achieve the low output impedance needed to drive the off-chip stage. The pixel buffer amplifiers are power cycled during the readout to further reduce the power budget of the readout circuit. Rows are only powered a few microseconds before their readout and the power is removed immediately after readout is completed. The fully differential off-chip driver is designed to directly drive the external ADCs at a readout frequency up to 40 MHz. This minimizes the number of components and the cost of the readout PCB.

The readout system (Figure 5) is composed of a single printed circuit board (PCB) which is organized around an Altera Cyclone V Field Programmable Gate Array (FPGA). The FPGA generates the control signals for the readout ASICs and receives the data stream from the 14 bit 40 MHz ADCs digitizing the multiplexed analogue output from the chips. Eight ASICs per module with 4 analog outputs per ASIC results in a total of 32 ADC channels. The data stream is reorganized such that contiguous images are formed and routed to a 10 Gigabit Ethernet (GbE) link for the data download to a receiving/storage server. This GbE data link can sustain frame rates in the 1 kHz range, well in excess of the 100 Hz machine repetition rate. A second 10 GbE connector is added to the PCB for applications in which the maximum frame rate of the ASIC-ADC combination (anticipated to be about 2.4 kHz) is desirable, e.g. in the synchrotron environment. A CM-BF537 system-on-a-board (SOB) (BlueTechnix, Vienna, Austria) is present on the module. The SOB controls the FPGA via an Asynchronous Memory Bus. The readout system also features a 100 Mbit Ethernet connection and runs a server that implements the configuration interface for the detector (slow control). Figure 6 displays a picture of the prototype JUNGFRÄU readout board.



## 2.4 Detector Integration

The integration of JUNGFRÄU into an experimental setup/beam line environment requires (concerning the hardware):

- $1 \times 10$  GbE link per module ( $2 \times$  for fast readout, not required for SwissFEL repetition rate),
  - 0.5 MPixel:  $1 \times 10$  GbE link,
  - 1 MPixel:  $2 \times 10$  GbE link,
  - 8 MPixel:  $16 \times 10$  GbE link,
  - 16 MPixel:  $32 \times 10$  GbE link,
- $1 \times 100$  MbE link to PSI network (independent of number of modules): Each module has a 100 MbE connection for the slow control. If a detector system consists of multiple modules, each module has its own 100 MbE connection. All the 100 MbE links from the modules are connected to one common switch, which in turn is connected to the PSI network via one single 100 MbE link. This switch is directly integrated with the multi-module detection system.
- $1 \times$  trigger input per detector system, LV-TTL signal on coaxial cable,
- $1 \times$  D-SUB 9 connection per detector system for the serial interface to receive the bunch-ID and time stamp,
- 220V power supply per detector system; the estimated power consumption is  $\approx 30$  W per module,
- Cooling water supply. A temperature controlled chiller with a cooling power in the range of 3 to 5 kW is required for big systems.

## 2.5 Prototypes

Two prototype ASICs have been designed: JUNGFRÄU 0.1 (Section 2.5.1) and JUNGFRÄU 0.2 (Section 2.5.2). The design of the first full ASIC, JUNGFRÄU 1.0, is completed, six wafers have been produced and testing of the JUNGFRÄU 1.0 chip is ongoing at present.

### 2.5.1 JUNGFRÄU 0.1

JUNGFRÄU 0.1 [17] is a small scale prototype (Figure 7, left) which has been designed and manufactured with a MPW run in October 2012. This chip is the first prototype designed in UMC 110 nm technology at PSI. A  $48 \times 48$  pixel matrix could be fit in the  $5 \times 5$  mm<sup>2</sup> available for the MPW, for a total active area of  $3.6 \times 3.6$  mm<sup>2</sup>. The chip is a small scale, fully functional readout ASIC designed as a demonstrator for the full size system.

### 2.5.2 JUNGFRÄU 0.2

The JUNGFRÄU 0.2 [20] prototype (Figure 7, right) consists of  $48 \times 48$  pixels and covers an area of about  $4 \times 4$  mm<sup>2</sup>. This chip is combined with a  $320 \mu\text{m}$  thick silicon sensor. Five different preamplifier variations are tested on the JUNGFRÄU 0.2 prototype chip. Rows 1-6, rows 7-12, rows 13-24, rows 25-36 and rows 37-48 represent different variations of the JUNGFRÄU 0.2 prototype. The five variations were characterized and evaluated in detail. A report on the

performance of the different preamplifier circuits is beyond the scope of this report. Results reported on the single pixel performance relate to the preamplifier variation chosen for the final ASIC unless the performance of the entire chip is evaluated or stated otherwise.

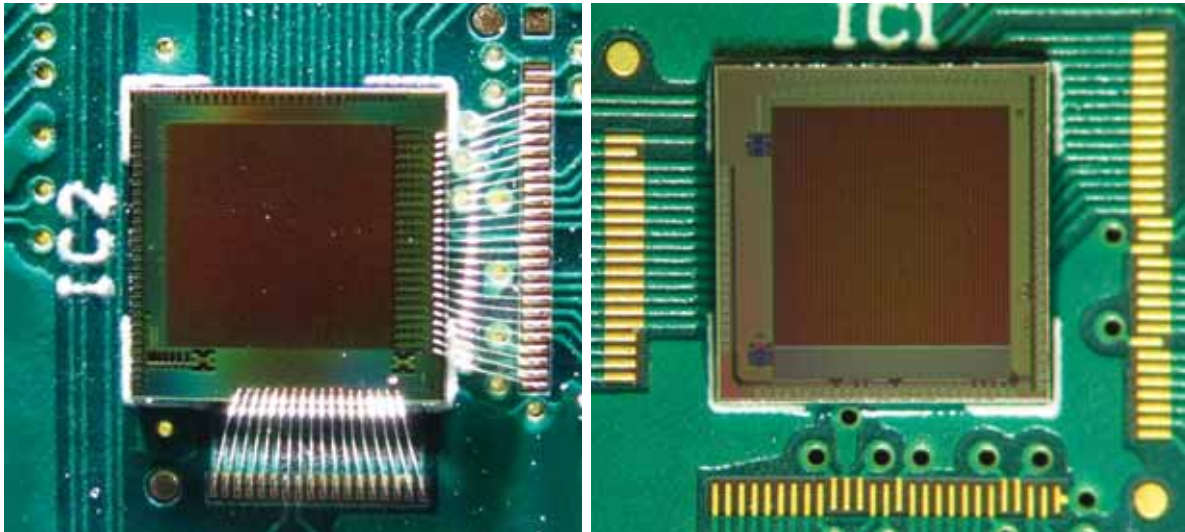


Figure 7: Pictures of the JUNGFRAU prototype chips: (left) JUNGFRAU 0.1, (right) JUNGFRAU 0.2.

### 3 Envisioned Systems for SwissFEL

Detector systems of different geometries and sizes are envisioned for the experimental stations at SwissFEL. An outline of the planned systems is given in this section. The interested reader is referred to the conceptual design reports of ES-A [4] and ES-B [5], respectively, for details of the scientific applications and the detailed realization of the experimental setups at the SwissFEL end stations.

#### 3.1 JUNGFRÄU for ES-A

ES-A requires two in-vacuum mounted detector systems [4]. In particular, a 16 MPixel system (32 JUNGFRÄU modules) for X-ray diffraction experiments is planned. This system will be mounted on-axis to the incident FEL beam that probes the sample. The detector system is constructed with a recess which accommodates the direct FEL beam and prevents damage to the detector system by the direct incidence of the FEL beam. In addition, ES-A requires an 8 MPixel system (16 JUNGFRÄU modules) for the construction of a X-ray emission spectrometer, in which JUNGFRÄU will be incorporated to detect X-ray fluorescence photons. This system will also be mounted in-vacuum in the form of an elongated “strip” (Figure 8).

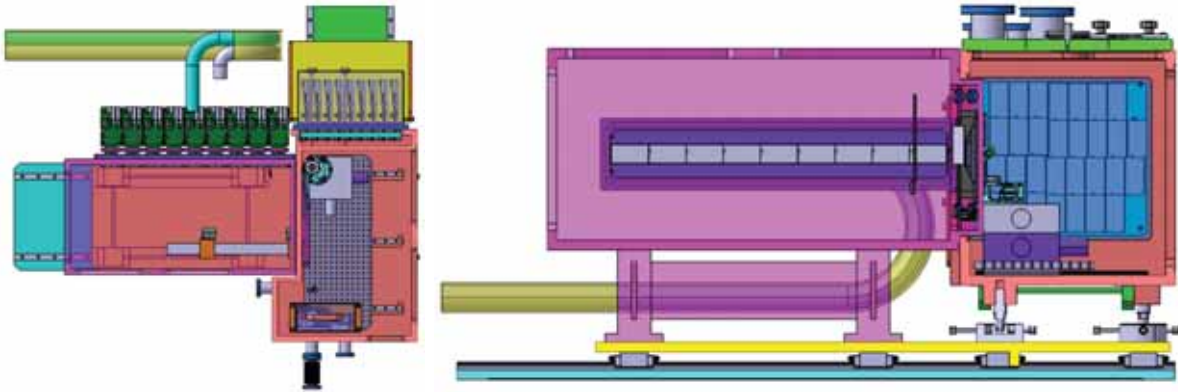


Figure 8: Drawings of a possible implementation of the two JUNGFRÄU in-vacuum systems for ES-A. The figures show a top view (left) and vertical (right) cut through the experimental setups for X-ray spectroscopy (chamber on left hand side) and X-ray diffraction (chamber on right hand side) experiments. The 16 MPixel system is located behind the sample interaction region at the end of the beam path in the right hand side chamber. The 8 MPixel system is integrated in the XES chamber wall with the sensitive detector surface inside the chamber and the readout electronics outside the chamber. The JUNGFRÄU modules are mounted one next to the other as to range over the entire back side of the chamber. Figure courtesy Jerome Stettler and Lukas Schaedler.

#### 3.2 JUNGFRÄU for ES-B

ES-B requires a 16 MPixel system (32 JUNGFRÄU modules) for the trXRD experimental setup. The ES-B system will be mounted in-air on a robot arm which will be able to position the pixel detector at different angles and distances from the sample under study. This multi-module system will be constructed around a central recess. A single JUNGFRÄU module will be used for experiments which require the detector to be located close to the sample.

### 3.3 JUNGFRAU for SwissFEL “Pool”

Another two 1 MPixel systems, i.e. 2 JUNGFRAU modules each, are reserved for various detection tasks at SwissFEL.

### 3.4 JUNGFRAU Production

Currently, the construction of 85 modules is required for SwissFEL.

- ES-A: 16 MPixel for XRD  $\rightarrow$  32 modules
- ES-A: 8 MPixel for XES  $\rightarrow$  16 modules
- ES-B: 16 MPixel for trXRD  $\rightarrow$  32 modules
- ES-B: 0.5 MPixel for trXRD  $\rightarrow$  1 module
- SwissFEL general:  $2 \times 1$  MPixel  $\rightarrow$  4 modules

The production of JUNGFRAU detector modules is planned based on an estimated production yield of about 80-90%.

## 4 Characterization Results

Selected characterization results from both JUNGFRAU 0.1 and JUNGFRAU 0.2 are presented with a focus on characterization results from the second JUNGFRAU prototype chip. In particular, ASIC characterization results as well as detector tests from the hybridized chip under white visible light, fluorescence X-ray, infrared (IR) laser and synchrotron irradiation are presented.

### 4.1 Noise Performance and Photon Detection at Low Energies

The noise performance of the JUNGFRAU 0.2 ASIC is evaluated with the pixels preamplifiers in high gain mode. Noise measurements are performed in the absence of photon irradiation. Prior X-ray fluorescence irradiation measurements are typically employed to establish the gain of each pixel in units of eV/ADC (analog-to-digital converter). The relationship of 3.6 eV/electron-hole-pair in silicon sensors is then employed to express the noise performance of the ASIC in terms of the equivalent noise charge (e.n.c.) in the units of “electrons” ( $e^-$ ).

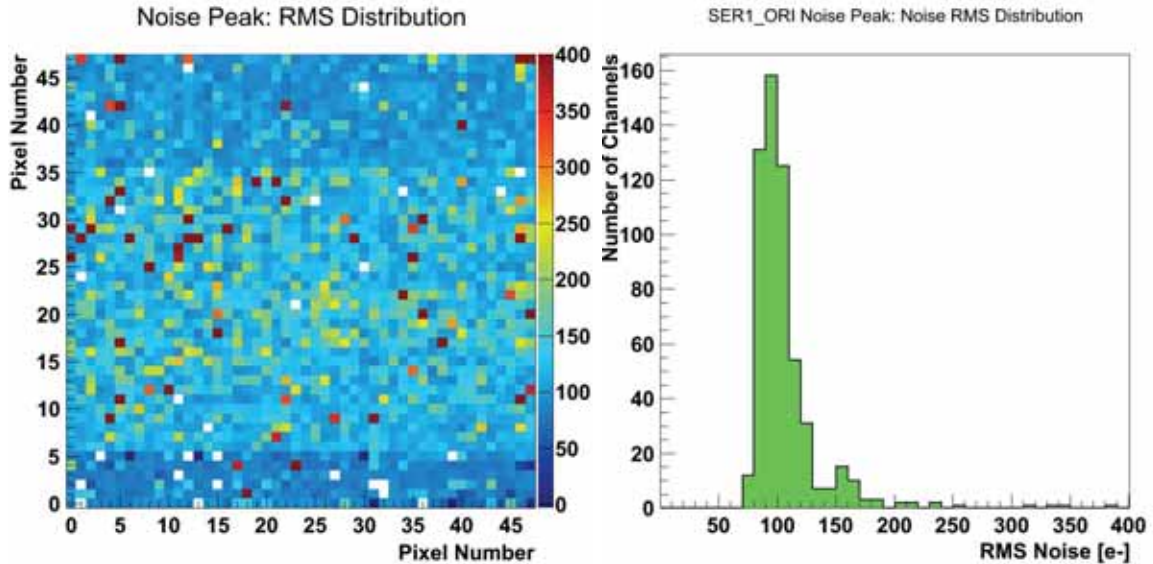


Figure 9: JUNGFRAU 0.2 r.m.s. noise in high gain mode. (left) 2D noise map. (right) Histogram of the noise distribution. The selected preamplifier variation corresponds to row 36-48 on the prototype chip.

The root-mean-square (r.m.s.) of the pixel noise is computed by a Gaussian fit to the noise peak, i.e. the pixel output signal in the absence of photon signal. Figure 9 displays the noise performance of the JUNGFRAU 0.2 ASIC. The two-dimensional noise map displays each pixel’s noise. The histogram shows the r.m.s. distribution of the pixel noise for the preamplifier variation chosen for the final JUNGFRAU ASIC. The noise distribution for JUNGFRAU 0.2 peaks around  $100 e^-$  ( $70-140 e^-$ ) but shows a few pixels in a tail towards higher r.m.s. noise ( $> 150 e^-$ ). This tail can be attributed in part to random telegraph noise (RTN) signal [21] and to a few noisy pixels. The main contribution to the pixel noise is given by the pixel preamplifier (80%), while the readout chain and the correlated double sampling stage are measured to share the remaining noise contributions.

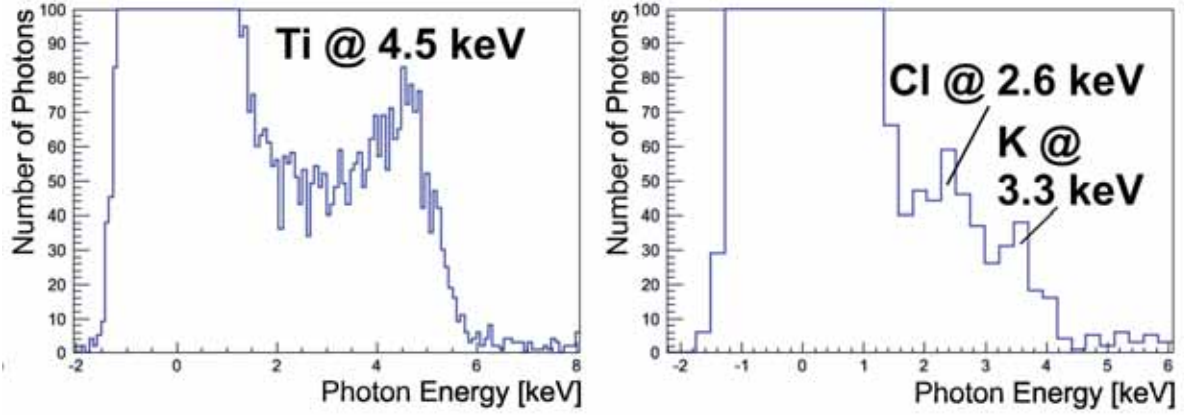


Figure 10: JUNGFRAU low X-ray energy spectra. The noise peak spans the energy range  $< 2$  keV. (left) Zoom on the X-ray spectrum from fluorescence irradiation of titanium at 4.5 keV and (right) from chlorine at 2.6 keV and potassium at 3.3 keV. The noise peak spans the energy range below 2 keV. Different acquisition times and the number of acquisition frames for the left versus the right panels change the appearance of the noise peak.

A pixel r.m.s. noise of  $100 e^-$  corresponds to about  $100e^- \times 3.6\text{eV}/e^- = 360$  eV photon energy in our system. A detection system with such a noise performance can reliably measure photon signal down to at least 2 keV when assuming a five sigma statistical margin ( $\sigma = 360$  eV,  $5 \times \sigma = 1800$  eV  $< 2$  keV). The “low energy” performance of JUNGFRAU 0.2 is evaluated in fluorescent X-ray irradiation experiments with fluorescence photons from an elemental sample of titanium ( $K\alpha(\text{Ti}) \approx 4.5$  keV) and a crystalline sample of potassium chloride ( $K\alpha(\text{K}) \approx 3.3$  keV,  $K\alpha(\text{Cl}) \approx 2.6$  keV). The resulting X-ray spectra are displayed in Figure 10, where the X-ray fluorescence peaks of titanium, potassium and chlorine are clearly separated from the noise peak.

The noise performance of JUNGFRAU 0.2 is also investigated over an input signal range equivalent to 1 up to  $10^4$  12 keV photons. The automatic gain switching circuit is enabled in this measurement. The test is performed by illumination of the entire pixel matrix with white visible light from a light bulb. The aluminum entrance window on top of the sensor is etched away for this measurement. The integration time of the pixels is gradually prolonged to increase the amount of input signal to the system. The measured output-versus-time characteristic, i.e. the ADC output versus the integration time, in the high gain stage combined with the eV/ADCU conversion factor enables to transform the integration time to integrated charge in the unit of 12 keV photons. Initially at low input signals, the pixels are in the high gain stage. The pixels switch to the medium gain stage around an input charge equivalent to 30 12 keV photons and to the low gain stage around an input charge of about 700 12 keV photons (Figure 11, see [17] for a similar measurement).

The r.m.s. noise of the pixels (in units of 12 keV photons) is computed for the entire dynamic range and compared to the expected Poisson fluctuation ( $\sqrt{N}$ ) in the number of input photons  $N$  (Figure 11 (bottom)). Importantly, the noise performance for all three gain stages is well below the Poisson fluctuation. This represents the optimal noise prerequisite for JUNGFRAU since the detection is limited by photon statistics rather than by the detector noise.

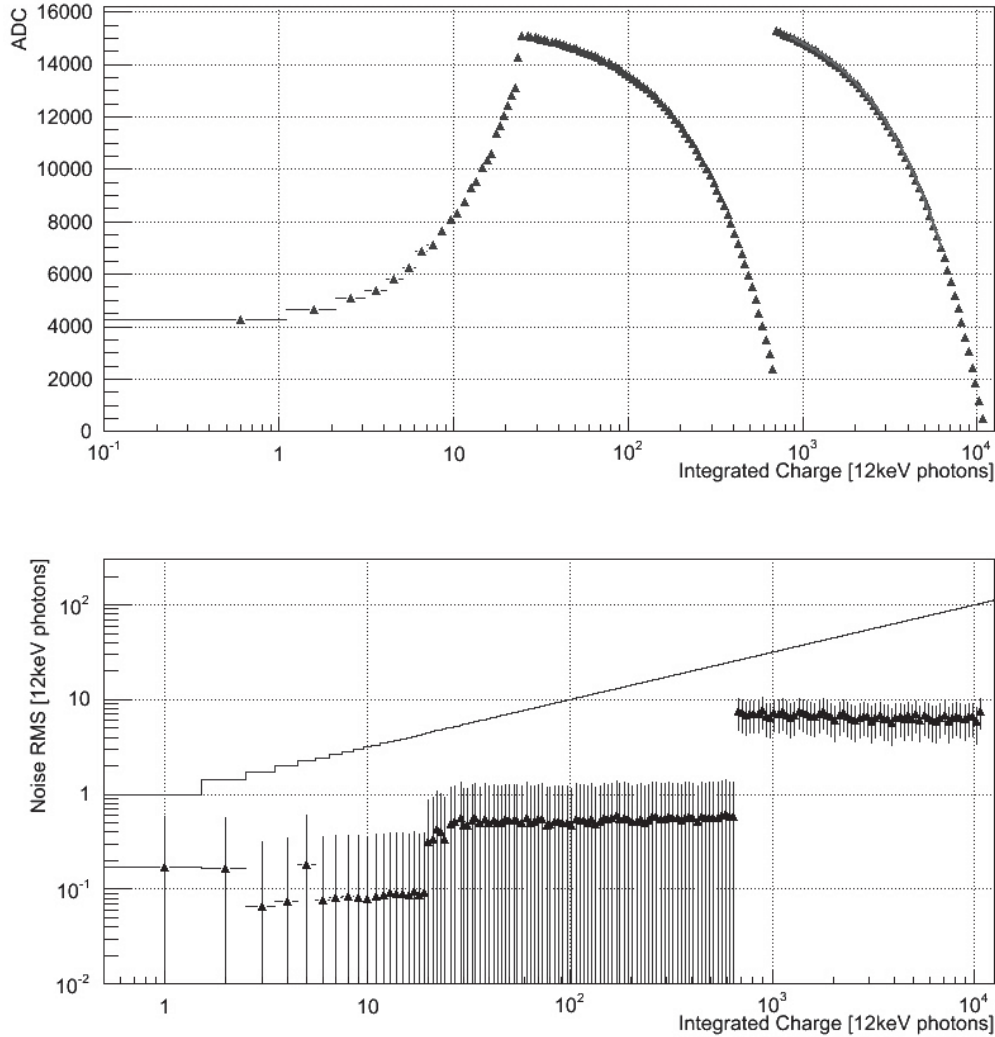


Figure 11: (top) The output characteristic of a JUNGFRAU 0.2 pixel over an input signal range corresponding to 1 up to  $10^4$  12 keV photons (details of measurement in text). The measured output-versus-photon number characteristic (x-axis on logarithmic, y-axis on linear scale) is used to extract the calibration parameters (i. e. the offset and the slope of the curve) for the three gain stages of the JUNGFRAU preamplifier. These calibration parameters in combination with the gain bits are employed in the analysis to convert the charge integrated in the preamplifier to the actual number of photons registered by a pixel. (bottom) Noise performance of the three gain stages of the JUNGFRAU 0.2 prototype chip over an input signal range corresponding to 1 up to  $10^4$  12 keV photons (both axes on logarithmic scale). The line indicates the Poisson fluctuation of the photon input signal.

## 4.2 Photon Detection above 10 keV

Examples of X-ray detection in the photon energy range above 10 keV are displayed in Figure 12. In these experiments, the system is flat-field illuminated by synchrotron light at 10, 16 and 20 keV (Synchrotron Radiation for Medical Physics (SYRMEP) beam line, Elettra Sincrotrone, Trieste, Italy [22]). The photon flux is adjusted such that not more than one photon per acquisition time impinges on a given pixel. JUNGFRUAU 0.2 is operated in high gain mode and about  $1.6$  to  $2 \cdot 10^5$  frames are acquired per photon energy. Acquisition times of  $1 \mu\text{s}$  (16 keV) and  $50 \mu\text{s}$  (10 keV and 20 keV) are employed. The resulting X-ray spectra of one selected pixel are displayed in Figure 12. The spectra are rebinned by a factor of 10.

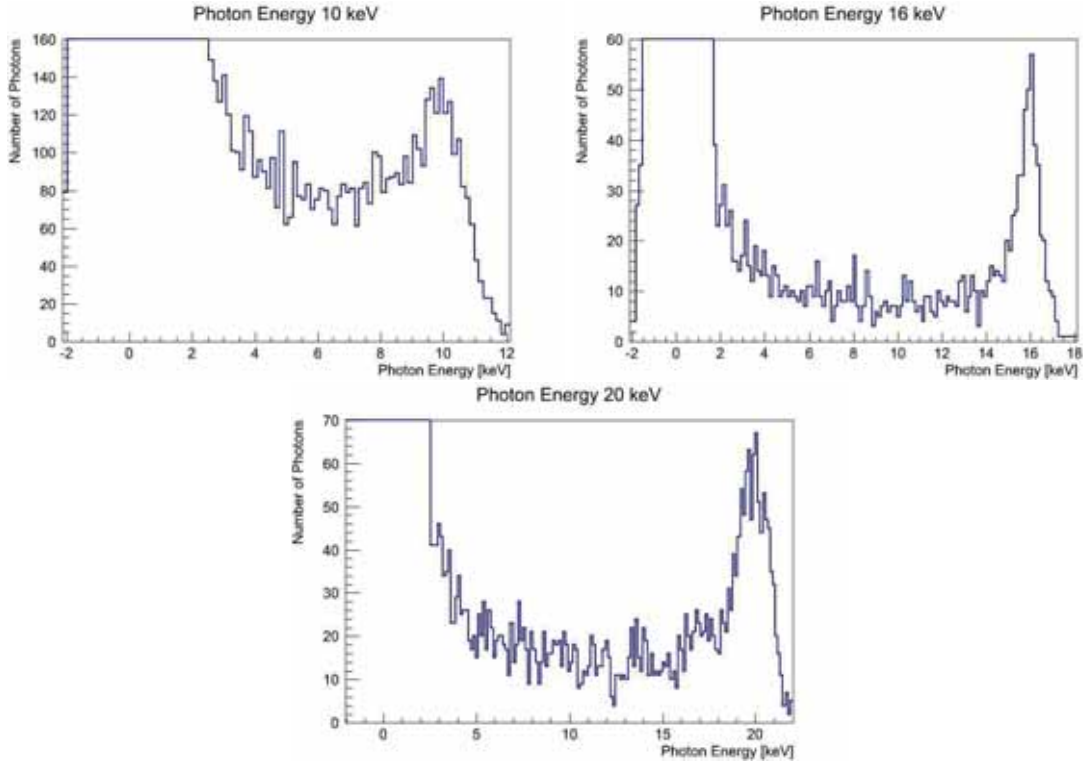


Figure 12: X-ray spectra at photon energies of (top left) 10 keV, (top right) 16 keV, (bottom) 20 keV, respectively.

## 4.3 Gain

The gain distribution of the ASIC is determined by illumination of the system with photons of a known energy. The pulse height distribution of each pixel is fit and the pixel gain in ADC units (ADCu) is extracted and computed in terms of ADCu/keV. Figure 13 shows the 2D gain map of JUNGFRUAU 0.2 when operated at medium gain (left) and at high gain (right). Clearly, the five preamplifier versions can be identified as horizontal zones of different gain performance in the ASIC. The gain is stable and displays little variation (around 3%) throughout each individual preamplifier variation.

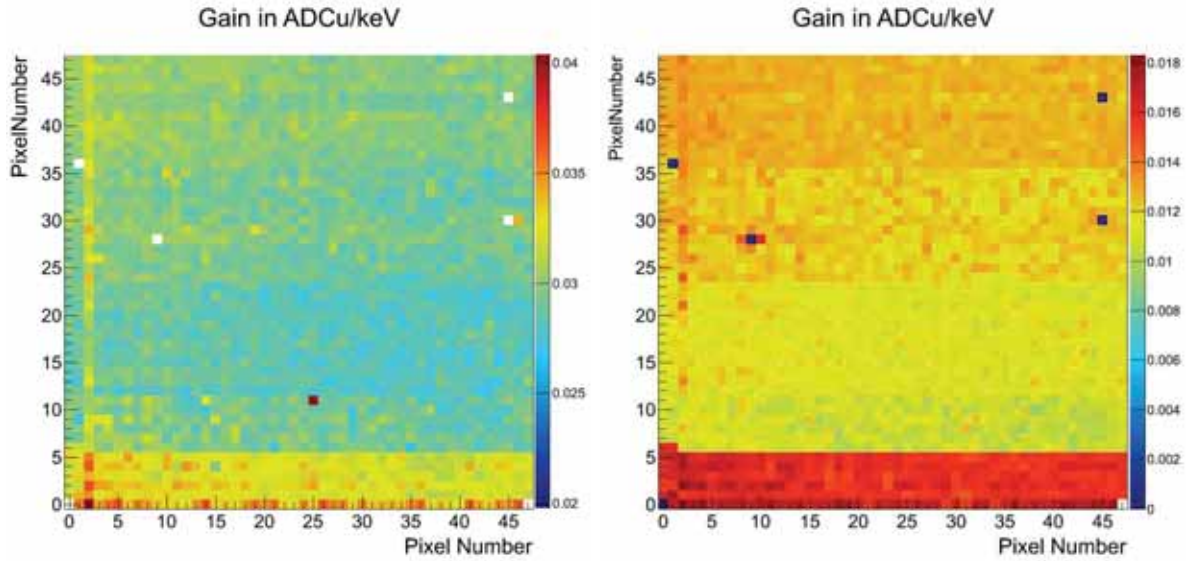


Figure 13: 2D gain maps of JUNGFRAU 0.2. (left) Gain map at medium gain, 16 keV photons, acquisition time  $1 \mu\text{s}$ . (right) Gain map at high gain, 20 keV photons, acquisition time  $50 \mu\text{s}$ .

#### 4.4 Linearity of the Pixel Response

The expected number of photons is deduced from a fit to the measured pixel output in gain switching mode, from which the gain stage slope and offset are extracted (Section 4.1 and Figure 11). The linearity error of the pixel response is established to be within  $\pm 1\%$  for the dynamic range of JUNGFRAU (Figure 14).

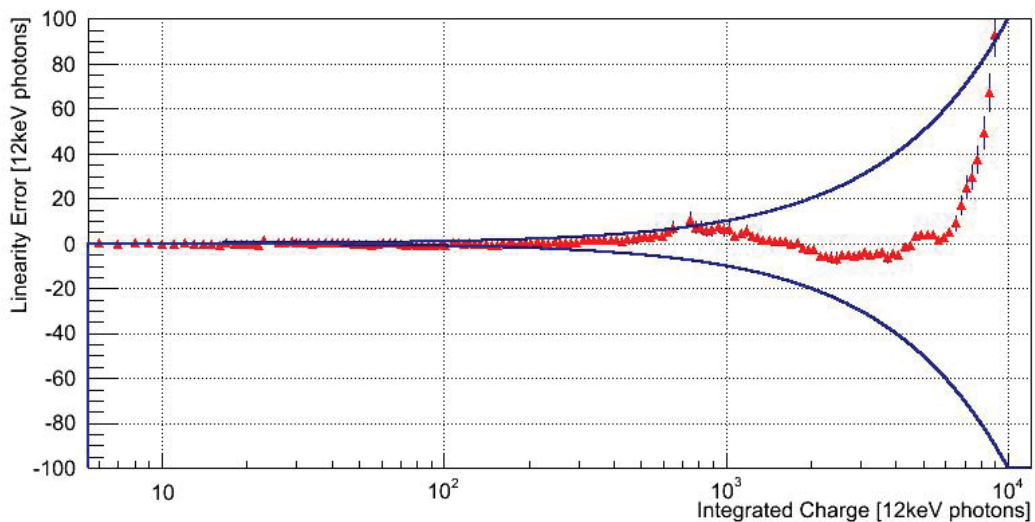


Figure 14: The linearity error of the pixel response is displayed (red, linear scale) as a function of the integrated charge (logarithmic scale). The blue lines indicate a linearity error of  $\pm 1\%$ . Since no gain bit is read out during this measurement and the analog information is ambiguous (i. e. the pixel switches or not depending on the noise), one data point is not analyzed at both gain transitions.

## 4.5 Speed

The measurement of the speed of the pixel electronics has two motivations. First, the reliable operation of the gain switching needs to be assessed for pulsed charge generation. In the measurement reported on up to this point, the charge is injected as a constant current distributed evenly over the entire integration time. Second, the time response puts a limit to the repetition rate at which the detector can be used. This is therefore an important parameter for applications at high repetition XFEL machines (as, for instance, the EU-XFEL) or for time-gated measurements at synchrotron sources.

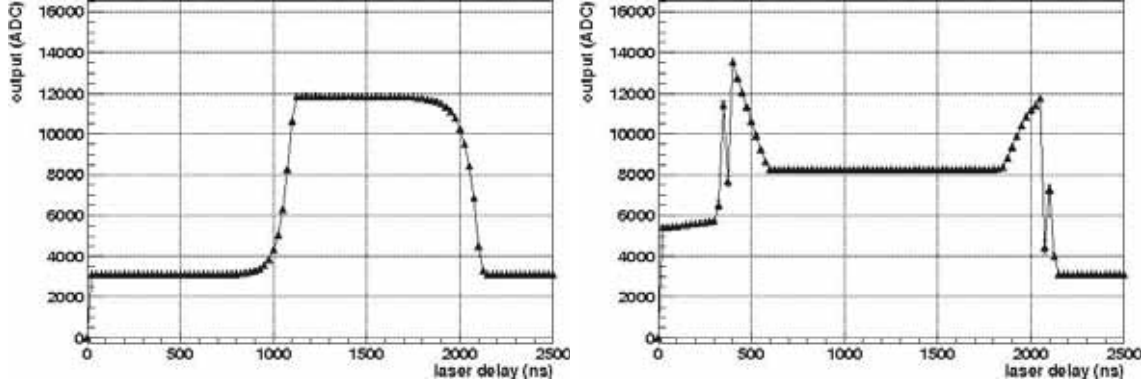


Figure 15: Output response of one JUNGFRAU 0.1 pixel as a function of the delay of the laser pulse with respect to the integration window: (left) in high gain and (right) when gain switching. The input intensity in the switching case is approximately 100 times higher than in the high gain one.

The measurement setup is based on a infrared diode laser (LDH-P-F-1030, PicoQuant, Berlin, Germany) with a maximum pulse intensity of 200 pJ and pulse duration of 5 ps. The diode output is coupled into an optical fiber which guides the light to an optical setup consisting of filter wheels, a beam expander and focusing lenses. Beam sizes as small as  $3 \mu\text{m}$  r.m.s. can be achieved on the sensor surface. A two filter wheel system for filter/attenuation selection enables to tune the beam intensity, and thus the number of electron-hole pairs created in the sensor, from 0 up to  $10^5$  12 keV photons equivalent charge.

The arrival time of the laser pulse has been changed in 25 ns steps with respect to a fixed  $1 \mu\text{s}$  integration window. The output intensity for the hit pixel has been measured for each delay step. The results for two different laser intensities are shown in Figure 15. In the left plot, the laser intensity is insufficient to trigger the automatic gain switching circuit and the integration window is clearly visible as a plateau region on top of the offset level. The rise and fall times of the response curve are determined by the response of the CDS stage (the slowest link in the chain) and are on the order of 100 ns (10% to 90%). If the signal is more intense and the automatic gain switching logic is triggered, the response is more complex both due to the gain switching itself and the bypassing of the CDS buffer.

Note that a wide and flat signal plateau is achieved independent of the effects during the transients both in the low and high intensity case. A total readout cycle (reset-integration-storage) of  $1.5 \mu\text{s}$  is feasible.

## 4.6 Imaging Measurements

### 4.6.1 High Dynamic Range Imaging Via Gain Switching

High dynamic range imaging enabled by the dynamically gain switching pixel preamplifiers is demonstrated by infrared laser illumination. In this experiment, an IR laser beam (diameter set to 25 pixels) is directed on the pixel sensor. The photon flux is adjusted such that the detector dynamic range of four orders of magnitude is spanned throughout the illuminated spot. The highest IR photon flux is deposited at the center of the laser distribution which displays an approximately Gaussian beam profile. Different pixels range in different preamplifier gain stages.

Experimentally, the three gain stages are observed in the “analog” pixel output plot (Figure 16, top left). Little and/or only noise input signal is registered (color-coded in blue) in areas on the chip where no IR photons are impinging. Towards the center of the analog image, the registered signal input increases up to the maximum 14-bit ADC values of the pixels in the high gain stage (maximum indicated by red color). Then, the gain switches to the medium gain stage which is characterized by a negative gain slope (colors red to blue). Again, the gain switches and the distribution is described by the negative gain slope of the low gain stage (colors red to blue, maximum of distribution indicated by yellow color). The gain stage information is encoded in the gain bits and is schematically displayed in Figure 16 (top right) where pixels colored white are in the high gain stage (low input signal up to the equivalent of about 30-12 keV photons), where green encodes the medium gain stage (signal equivalent to about 30-700-12 keV photons) and where red stands for the low gain stage (signal > 700-12 keV photons) (Figure 11).

A “photon image” with the number of photons registered per pixel is calculated via a charge-to-photon calibration as outlined in Section 4.1 and Figure 11. Figure 16 (bottom) displays the reconstructed number of 12 keV photons registered per pixel on a linear and logarithmic scale, respectively. The inset in Figure 16 (bottom left) shows a slice through the center of the beam distribution. The analog pixel output, the gain bit distribution and the reconstructed number of photons per pixel qualitatively coincide with the expected nearly Gaussian laser beam profile. An additional imaging experiment in gain switching mode with the IR laser involves the placement of a metal mask with sharp edges and clearly defined features in front of the chip. The experiment establishes that the mask pattern is accurately imaged on the chip and that there is no “gain switching” crosstalk between pixels (Figure 17 right). In a similar experiment, a step attenuator, i.e. an attenuator of several different thicknesses of aluminum is placed in front of the chip and the system is illuminated by synchrotron light at 12 keV (SYRMEP beam line). Also here, the gain switching works successfully over four orders of magnitude of input signal and data in units of “photons per pixel” can be extracted (Figure 17 left).

Importantly, these experiments demonstrate automatic gain switching over the chips specified dynamic range of input signal as shown for visible light, IR laser and synchrotron illumination. The performance is flawless whether the input signal is concentrated on part of the chip or if the chip is entirely flooded by photons for this prototype chip.

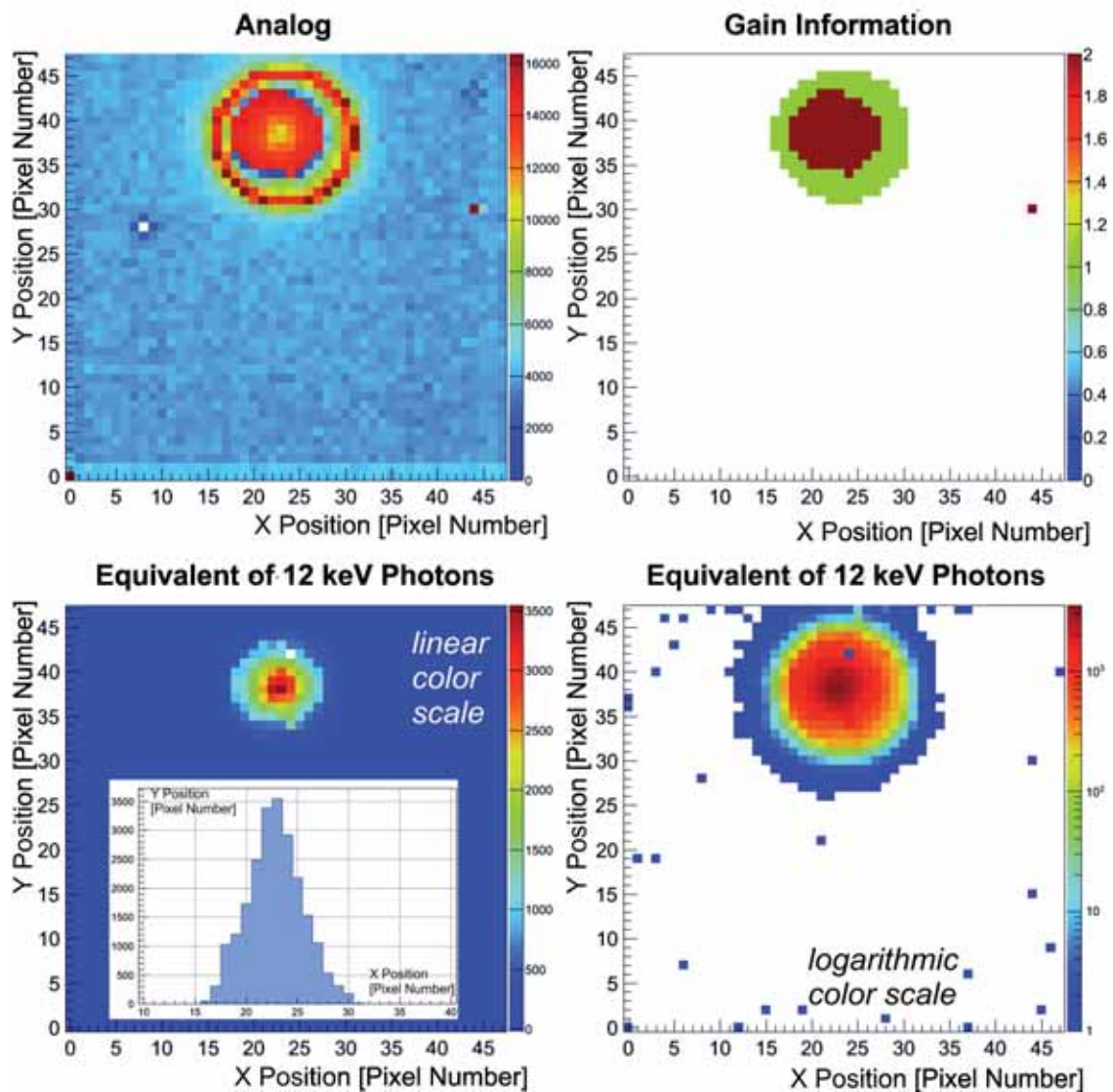


Figure 16: IR laser irradiation and dynamic gain switching. (top left) Analog signal output from 14-bit ADC, (top right) according gain bit information (0=high gain, 1=medium gain, 2=low gain), (bottom left) number of 12 keV photons per pixel displayed on a linear color scale and projection through the center of the beam distribution in the x-direction (inset), (bottom right) number of 12 keV photons per pixel shown on a logarithmic color scale.

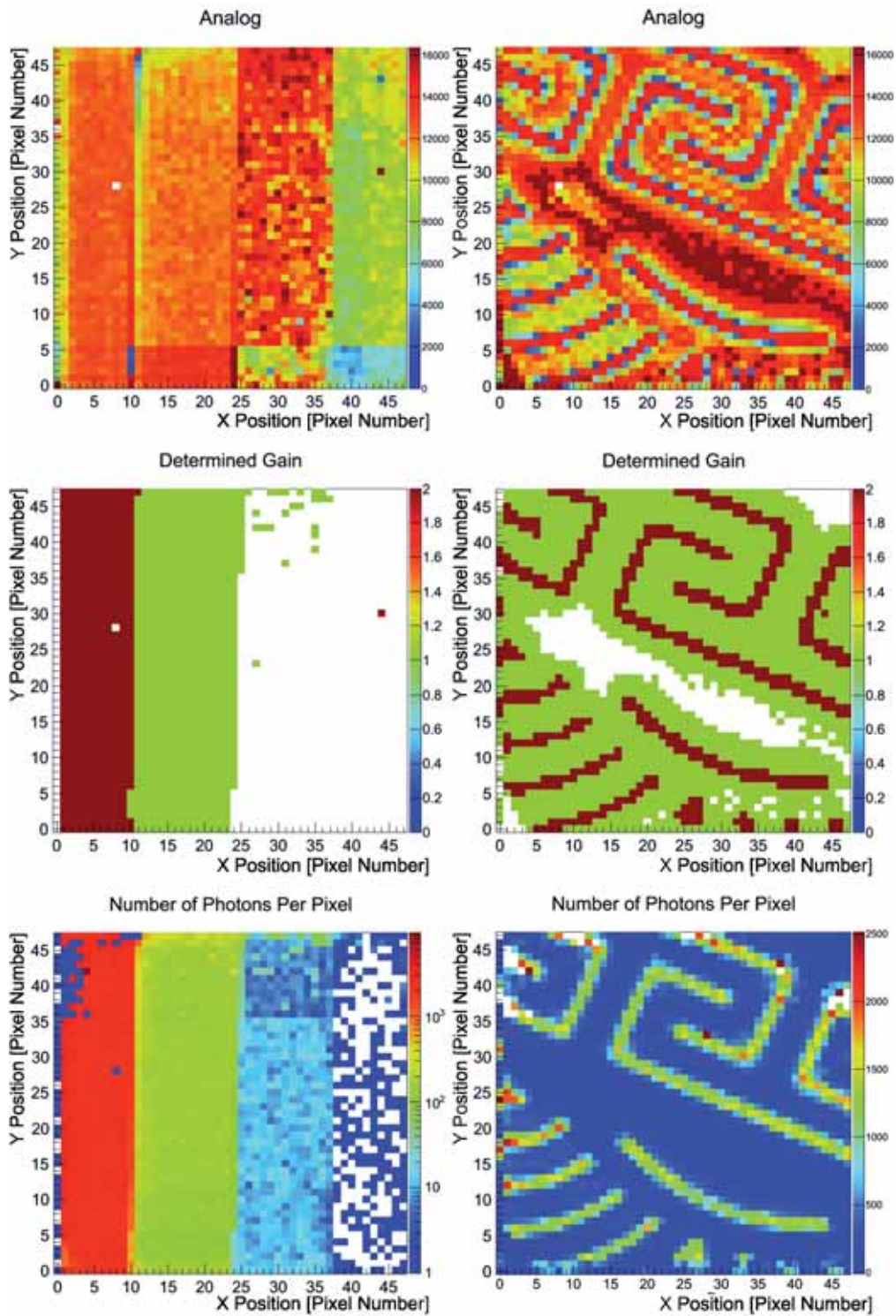


Figure 17: Dynamic gain switching (left) at four different photon intensities at the synchrotron and (right) with an IR laser through a metal mask. (top row) Analog signal output from 14-bit ADC, (middle row) according gain bit information (0=high gain, 1=medium gain, 2=low gain), (bottom row) number of 12 keV photons per pixel.

## 4.6.2 Spatial Imaging Resolution

The spatial imaging resolution of the JUNGFRAU 0.2 prototype chip is investigated by the placement of a sharp edge stainless steel attenuator in front of the chip. The system is illuminated by synchrotron light at 12 keV (SYRMEP beam line). The chip is set to high gain mode and  $5 \cdot 10^5$  frames of  $20 \mu s$  acquisition time are acquired. Figure 18 (left) displays the accumulated number of photons per pixel for this measurement.

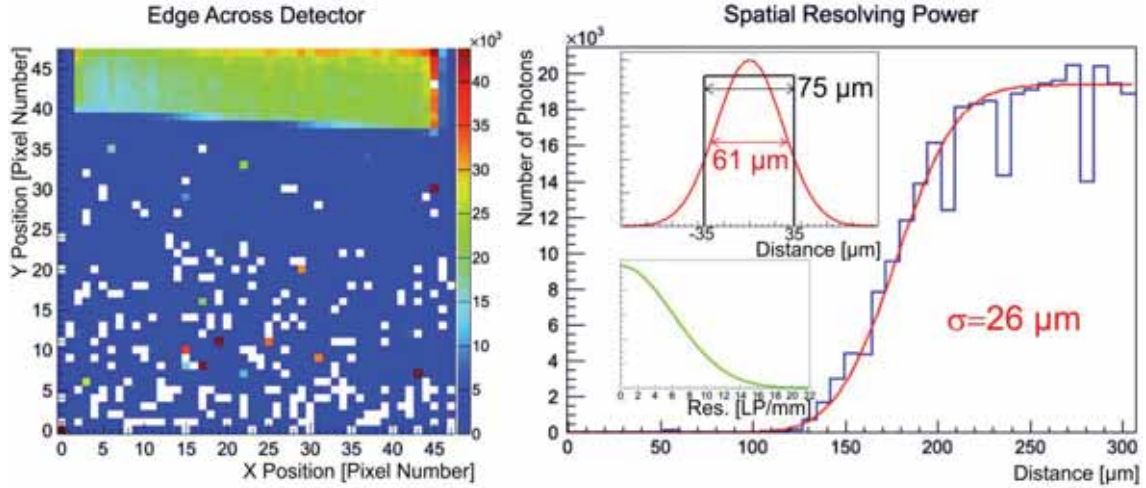


Figure 18: Edge spread function of the JUNGFRAU 0.2 chip. (left) A sharp edge is placed in front of the chip and the system is illuminated by synchrotron light at 12 keV. The bottom part of the chip is covered by the stainless steel edge and no/few photons are registered (encoded in dark blue or white color). The top part of the chip receives unattenuated photons (encoded in light blue to red color). (right) The edge spread function of the chip is displayed (blue) and fit with an error function (red). The top inset depicts the FWHM of the fit to the edge spread function of  $61 \mu m$  in comparison to the  $75 \mu m$  pixel size. The bottom inset displays the modulation transfer function, which indicates the spatial resolution of the detection system in the unit of line pairs per mm (LP/mm).

The sharpness of the edge imaged by the JUNGFRAU 0.2 prototype is analyzed. First, photon images are obtained for each acquisition frame via a charge-to-photon calibration as outlined in Section 4.1 and Figure 11. Then, the imaged edge is aligned with the pixel matrix in software. A finely binned histogram (1 bin =  $7.5 \mu m = 1/10$  pixel) that corresponds to a projection of the image along the edge axis is filled with the image points of the entire pixel matrix. Figure 18 (right) displays this point spread function (blue). An error function fit of this curve returns a standard deviation  $26 \mu m$  which is close to the theoretically expected binary resolution [23] of  $(pixel\ size) \sqrt{12} = 75 \mu m \sqrt{12} = 22 \mu m$ . The small deviation from the expected resolution is most likely due to charge sharing between neighboring pixels and a small noise contribution. The computed standard deviation of  $26 \mu m$  corresponds to a full-width at half maximum (FWHM) of  $FWHM = 2.35 \cdot 26 \mu m = 61 \mu m$  of the Gaussian point spread function, which is significantly smaller than the  $75 \mu m$  pixel size (Figure 18, right). The point spread function of the presented imaging system is outstanding and comparable magnitude to the spatial resolution delivered by single photon counting hybrid pixel detectors.

## 5 Project Milestones and Future Timeline

At this point, the JUNGFRAU 0.1 and JUNGFRAU 0.2 prototypes have been fully characterized and successfully tested. The design of the full JUNGFRAU 1.0 chip is completed, the according engineering run is completed and first JUNGFRAU 1.0 chips are under testing (Figure 19). Project milestones, the envisioned timeline and the current status of the tasks are displayed in Table 2.

Milestone	Completed By	Current Status
Tests & characterization of prototypes	January 2014	completed
ASIC design JUNGFRAU 1.0	June 2014	completed
JUNGFRAU 1.0 engineering run	September 2014	completed
JUNGFRAU 1.0 tested & characterized	March 2015	in progress
Readout system design	July 2014	completed
Module mechanics	November 2014	ongoing
1st detector system (500 kPixel)	May 2015	
1 MPixel/4 MPixel available	August 2015	
16 MPixel available	December 2016	

Table 2: Milestones of the JUNGFRAU project, envisioned timeline and current status.

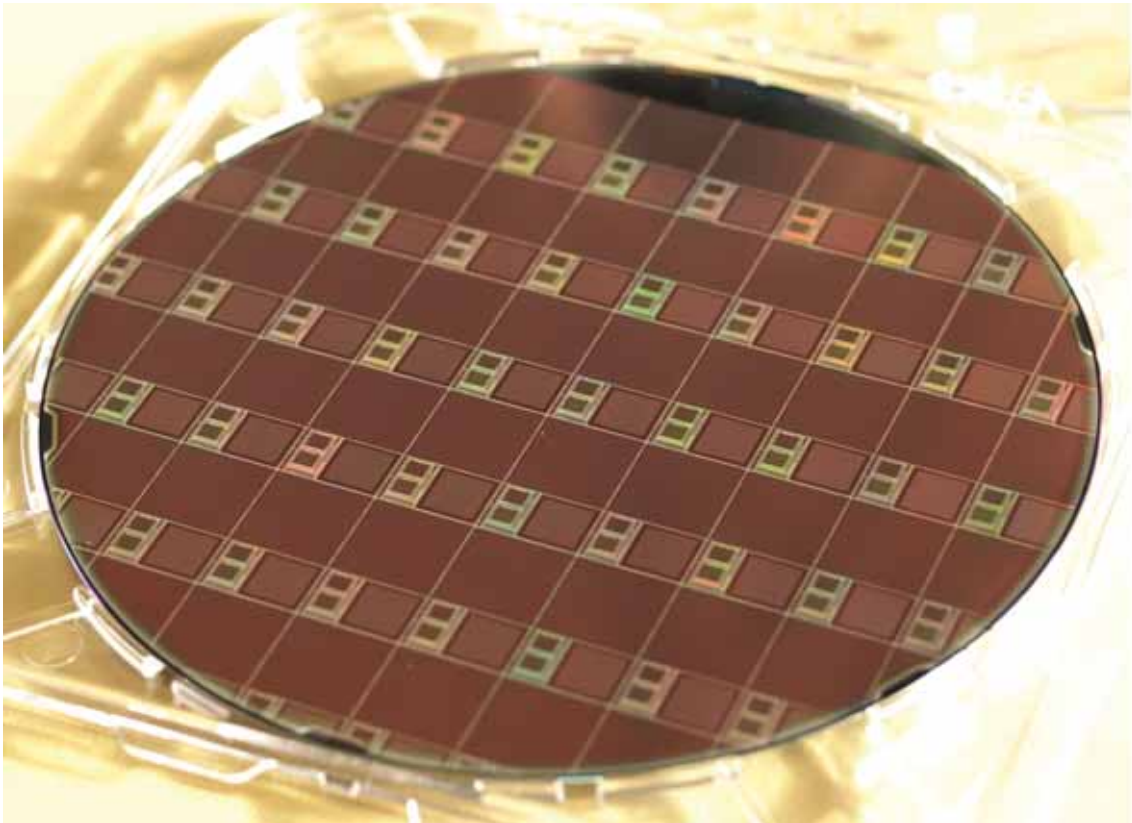


Figure 19: JUNGFRAU 1.0 wafer from the 2014 engineering run. Besides the JUNGFRAU 1.0 chips, the picture shows smaller (prototype) chips and test structures on the wafer.

## 6 The JUNGFRÄU Team

JUNGFRÄU is developed by the Swiss Light Source Detector Group. Table 3 provides the core JUNGFRÄU team members, associated tasks and contact information.

Task	Person	Email Address ...@psi.ch
ASIC Design/Project Overall	Aldo Mozzanica	aldo.mozzanica
Group Leader	Bernd Schmitt	bernd.schmitt
Characterization/Calibration	Julia Smith	julia.smith
Mechanical Design	Lukas Schaedler	lukas.schaedler
Readout Electronics Design	Christian Ruder	christian.ruder

Table 3: Core JUNGFRÄU team, tasks and contact details.

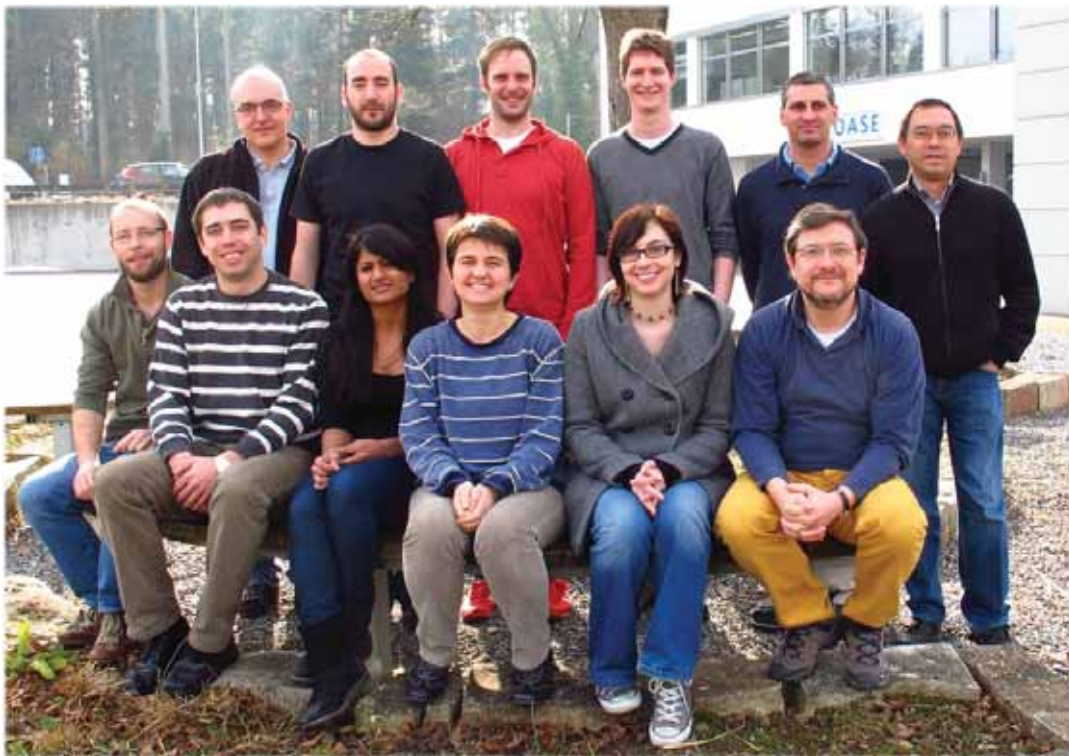


Figure 20: SLS Detector Group (picture March 2013). Back row: Bernd Schmitt, Christian Ruder, Dominic Greiffenberg, Sebastian Cartier, Ian Johnson, Xintian Shi. Front row: Aldo Mozzanica, Lukas Schaedler, Dhanya Maliakal, Anna Bergamaschi, Gemma Tinti, Roberto Dinapoli. Not in picture: Davide Mezza, Julia Smith.

## 7 Concluding Remarks and Outlook

JUNGFRAU is a two-dimensional imaging detector for photon science at X-ray free electron lasers, in particular SwissFEL, and high count rate synchrotron radiation research. The work presented in this paper has shown that JUNGFRAU is a successful charge-integrating, dynamic gain switching hybrid pixel detector, which provides single photon sensitivity and a high dynamic range of input signals in excess of  $10^4$  photons/pulse/pixel. JUNGFRAU will provide frame rates in excess of 2 kHz which will result in linear count rate capabilities of 25 MHz/pixel. JUNGFRAU's noise performance is established to be around 100 electrons and well below the Poisson photon number fluctuation over the entire dynamic range. The pixel response is linear to within  $\pm 1\%$  over the full dynamic range of four orders of magnitude of input signal. The X-ray energy range from 2 keV is accessible at single photon resolution. A high spatial resolving power comparable to single photon counting systems is demonstrated.

The design of the first full ASIC, JUNGFRAU 1.0, is completed. Performance testing on JUNGFRAU 1.0 will follow research lines similar to the work of this report and of [17, 20] and will be performed at the beginning of 2015. In addition, ASIC characterization in terms of radiation hardness is envisioned, i.e. all performance tests will be repeated after an X-ray irradiation equivalent to several years of SwissFEL operation. Proof-of-performance experiments at synchrotron and XFEL sources are planned. Other aspects of future work include protocol development for accurate and stable charge-to-photon calibrations such that the users of JUNGFRAU detection systems will receive output data in terms of “number of photons per pixel”. Module production for various experimental setups at the SwissFEL experimental stations and at synchrotron light sources is planned for 2015. The mechanical design of JUNGFRAU modules and the design of the implementation of JUNGFRAU systems at ES-A and ES-B are currently ongoing and are expected to continue throughout 2015.

In conclusion, the presented JUNGFRAU detection systems will give the SwissFEL user community the opportunity to fully exploit the scientific capabilities opened up by this novel light source.

### Further Information

- JUNGFRAU on the PSI website: <http://www.psi.ch/detectors/jungfrau>
- A. Mozzanica, A. Bergamaschi, S. Cartier et al., *Prototype Characterization of the JUNGFRAU Pixel Detector for SwissFEL*, JINST, 9, C05010, 2014
- J. H. Jungmann-Smith, A. Bergamaschi, S. Cartier et al., *JUNGFRAU 0.2: Characterization of a Gain-Switching, High Dynamic Range Imaging System for Photon Science at SwissFEL and Synchrotrons*, JINST, 9, P12013, 2014

### Acknowledgements

The authors acknowledge valuable contributions of all Swiss Light Source Detector Group members to the project (in particular Christian Ruder and Lukas Schaedler), the collaboration with the AGIPD consortium and the experimental staff of the SwissFEL experimental stations.

## References

- [1] B. D. Patterson, R. Abela, H. H. Braun et al., *Coherent Science at the SwissFEL X-Ray Laser*, New J. Phys., 12, 035012, 2010
- [2] SwissFEL *Conceptual Design Report*, 2010
- [3] B. D. Patterson, *Ultrafast Phenomena at the Nanoscale, Science Opportunities at the Swiss-FEL X-Ray Laser*, PSI Bericht Nr. 09-10, 2009
- [4] C. J. Milne, *SwissFEL Experimental Station A: Conceptual Design Report*, 2013
- [5] G. Ingold, P. Beaud, *SwissFEL Experimental Station B: Conceptual Design Report*, 2013
- [6] C. Broennimann, E. F. Eikenberry, B. Henrich et al., *The PILATUS 1M Detector*, J. Synchrotron. Radiat., 13, 120, 2006
- [7] R. Dinapoli, A. Bergamaschi, B. Henrich et al., *EIGER: Next Generation Single Photon Counting Detector for X-Ray Applications*, Nucl. Instrum. Meth. A., 650, 11, 79-83, 2011
- [8] M. Campbell, *10 Years of Medipix2 Collaboration*, Nucl. Instrum. Meth. A., 633, S1-S10, 2011
- [9] P. Hart, S. Boutet, G. Carini et al., *The CSPAD Megapixel X-Ray Camera at LCLS*, Proc. SPIE 8504, X-Ray Free-Electron Lasers: Beam Diagnostics, beam line instrumentation, and applications, 85040C, 2012
- [10] J. Arthur, G. Materlik, R. Tatchyn et al., *The LCLS A 4th-Generation Light-Source Using the SLAC Linac*, Rev. Sci. Instrum., 66, 2, 1987-1989, 1995
- [11] P. Goettlicher, H. Graafsma, H. Hirsemann et al., *The Adaptive Gain Integrating Pixel Detector (AGIPD): A detector for the European XFEL. Development and Status.*, IEEE Nucl. Sci. Symp. Conf. Rec. 2009, -5, 1817-1820, 2009
- [12] A. Blue, M. French, P. Seller et al., *Edgeless Sensor Fevelopment for the LPD Hybrid Pixel Detector at XFEL*, Nucl. Instrum. Meth. A., 607, 1, 55-56, 2009
- [13] M. Porro et al., *Development of the DEPFET Sensor with Signal Compression: A Large Format X-ray Imager with Mega-Frame Readout Capability for the European XFEL*, IEEE Nucl. Sci. Symp. Conf. Rec. 2011, 1424-1434, 2011
- [14] *EU-XFEL*, Hamburg, Germany
- [15] C. Saji, T. Ohata, T. Kudo et al., *Evaluation of Data-Acquisition Front Ends for Handling High-Bandwidth Data from X-Ray 2D Detectors: A Feasibility Study*, Nucl. Instrum. Meth. A., 731, 229-233, 2013
- [16] D. Pile, *X-Rays First Light from SACLA*, Nature Photon., 5, 8, 456-457, 2011
- [17] A. Mozzanica, A. Bergamaschi, S. Cartier et al., *Prototype Characterization of the JUNGFRÄU Pixel Detector for SwissFEL*, JINST, 9, C05010, 2014
- [18] G. Hülsen, Ch. Broennimann, E. F. Eikenberry and A. Wagner, *Protein Crystallography with a Novel Large-Area Pixel Detector*, J. Appl. Crystallogr., 39, 4, 550-557, 2006

- [19] A. Mozzanica, A. Bergamaschi, R. Dinapoli et al., *GOTTHARD Charge Integrating Read-out Detector: Design and Characterization*, JINST, 7, C01019, 2012
- [20] J. H. Jungmann-Smith, A. Mozzanica, A. Bergamaschi et al., *JUNGFRAU 0.2: Characterization of a Gain-Switching, High Dynamic Range Imaging System for Photon Science at SwissFEL and Synchrotrons*, JINST, 9, P12013, 2014
- [21] W. H. Card and A. Mavretic, *Burst Noise in Semiconductor Devices*, Second Annual Symposium on the Physics of Failure in Electronics, 268-283, 1963
- [22] A. Abrami, F. Arfelli, R. C. Barroso et al., *Medical Applications of Synchrotron Radiation at the SYRMEP Beamline of ELETTRA*, Nucl. Instrum. Meth. A., 548, 1-2, 221-227, 2005
- [23] L. Rossi, P. Fischer, R. Rohe et al., *Pixel Detectors, From Fundamentals to Applications*, Springer, 2006